BIOPHYSICS

# Penetration mechanics of a beetle intromittent organ with bending stiffness gradient and a soft tip

**Yoko Matsumura,* Alexander E. Kovalev, Stanislav N. Gorb**



**Hyper-elongated structures and their penetration are widespread among insects, for example, intromittent organs, ovipositors, and piercing-sucking mouthparts. The penetration of thin structures with high aspect ratio without buckling and rupturing is mechanically very challenging. However, this problem is economically solved in nature, and the solutions might be helpful for, for example, in the development of harmless catheters. We focus on the penetration process of a hyper-elongated structure of a cassidine beetle intromittent organ, termed a flagellum. We applied a three-point bending test for the flagellum to measure its bending stiffness along the entire flagellum. We demonstrated the bending stiffness gradient, in which the basal half is relatively stiff and the apical half is softer, whose good performance during copulation had been previously numerically demonstrated. The stiffness gradient is the result of the flagellum shape, which is cylindrical and tapered toward the tip. Moreover, the curved tip comprises a harder outer curve and a softer inner curve. Considering the findings of preceding studies, the flagellum works in the following way: (i) the bending stiffness gradient supports the flagellum, easily fitting to a shape of a highly coiled spermathecal duct, (ii) the stiffness property of the very tip may make the tip tougher, and (iii) the curled tip and homogeneously cylindrical shape of the organ help the very tip to fit the shape of the spermathecal duct of the female. Our study shows that the apparently simple flagellum penetration is achieved with numerous elaborate mechanical adaptations.**

## INTRODUCTION

Hyper-elongated penetration structures are widespread in animals, for example, (i) male intromittent organs especially in many insects [tables in the studies by Neufeld and Palmer (*1*) and Matsumura *et al.* (*2*)], (ii) female ovipositors in parasitic wasps (*3*, *4*), and (iii) insect mouthparts [acorn weeviles (*5*), butterflies (*6*), horse flies (*7*), and aphids and lac insect (*8*, *9*)]. The hyper-elongation of these chitinous cuticular structures results, in general, from the coevolutionary processes with functionally interacting structures. For example, the length of the male intromittent organ coevolved with that of the female spermathecal duct (*10*–*12*), the length of the fig wasp ovipositor coevolved with the thickness of egg-laying substrates (*3*), and insect mouthpart lengths coevolved with the sizes of host plants [acorn weevil rostrum and host seed sizes (*5*), butterfly proboscis and nectar site (*6*), and bug stylets and bark tissue thickness (*9*)].

Sometimes these elongated structures are extraordinarily long, a couple of times the body size. However, irrespective of the length of these structures, the animals can precisely control their movement to fulfill their original functions. Insertion and/or excavation of these hyper-elongated structures in nature are mechanically challenging, and the mechanics of these structures have just started to be theoretically and experimentally studied (*13*–*17*). Moreover, insertion of these structures is a highlighted topic in biomimetics and engineering fields with special focus on the prevention of buckling failure under compressive stress for medical applications (*18*, *19*) and in the medical field in terms of penile impotence or erectile dysfunction (*20*).

Here, we studied hyper-elongated intromittent organs that are longer than the male body size. This is found in many different animal groups (*1*), and the examples are most abundant in insects (*2*). In insects, the entire intromittent organ is usually stored in the abdomen (*21*). Therefore, males have to move the elongated structure for rather long distances to insert the elongated structure from their abdomen into a female duct, which is usually called spermatheca (or spermathecal duct). Although a tunnel-like structure, into which the elongated structure penetrates, is situated in the female, the correspondingly long female structures are convoluted and/or highly coiled (*10*, *22*–*25*) and penetration does not appear to be a very simple task for males. In addition, the elongated part of the intromittent organ seems to be very fragile [in an extreme case, its diameter is less than 2 μm (*24*)]. Nevertheless, breakage of the elongated structures does not often occur [0.8 to 3.4% of males of different earwig species (*26*), 1.0% of single-mated seed bug males, 22.5% of multiple-mated seed bug males (*27*), and 4.5% of field-collected females of a leaf beetle species had within a broken piece of the male intromittent organ (*24*)]. How do these animals achieve their challenging task without breaking their thin and seemingly fragile structures?

Filippov *et al.* (*13*, *14*) attempted to resolve this question with a numerical approach and used morphological data of the *Cassida* beetle system, whose insertion mechanism was previously studied in detail by Matsumura *et al.* (*25*). Males of the leaf beetles from the subfamily Cassidinae have a tube-like structure termed flagellum. It is generally long, sometimes reaching a length several times that of the body (*10*). The flagellum is situated in the lumen of the ejaculatory duct convoluted in the male abdomen (Fig. 1) (*25*). The ejaculatory duct unordinarily bears longitudinal muscles oriented along the duct, and their contraction results in pushing the flagellum out (*25*). Therefore, the penetration of the flagellum results from being pushed from its proximal end. This hypothetical mechanism had been numerically confirmed by Filippov *et al.* (*13*). Filippov *et al.* (*14*) showed that the gradient of material composition revealed in a confocal laser scanning microscope (CLSM) has a critically important role in establishing the gradient of mechanical properties and in enhancing insertion velocity. The hard intromittent organ with a soft apical part showed the best performance (*14*). It is known that male seed bugs with removed intromittent organ tips had reduced postcopulatory reproductive success (*28*). Change of the stiffness or stiffness gradient along the hyper-elongated intromittent organ, caused by tip breakage, is a likely reason for the male fitness reduction (*14*). However, the mechanics of male-and-female interactions are scarcely studied, although it is critically important to understand the

Department of Functional Morphology and Biomechanics, Zoological Institute, Kiel University, Am Botanischen Garten 1-9, D-24118 Kiel, Germany.
*Corresponding author. Email: yoko.matumura.hamupeni@gmail.com

coevolution of the male and female genitalia (*29*, *30*). In general, the mechanical properties of the genitalia are hardly investigated in invertebrates, so far with only one exception, that of *Leiobunum* harvestmen (*31*). Therefore, to clarify the mechanics of male and female genital interaction processes, we applied a three-point bending test for the *Cassida* beetle intromittent organ, which is ca. 10 mm in length (*13*) and <10 μm in diameter. We measured bending stiffness (flexural rigidity, *EI*; where *I* is the area moment of inertia and *E* is the Young's modulus) and material stiffness (Young's modulus) along the duct and tested whether the stiffness gradient exists along the duct as predicted in the preceding study (*14*). On the basis of the results of the flagellum mechanical properties, we discuss the male penetration mechanics.

## RESULTS

### Bending and material stiffness

We performed a bending test along the flagellum to measure absolute values of the flagellum stiffness ($n$ = 10; Fig. 2). The measurement was performed on 300-μm sections from the base to the tip, every second 300-μm section except for the very tip (ca. 200 μm) for each animal. On the basis of the images taken during the bending test (Fig. 3), we calculated the bending stiffness (Fig. 4, the black solid line). In general, the basal part of the flagellum shows higher bending stiffness values than its apical part.

The entire flagellum tube is cylindrical and becomes tapered from the base to the apex (Fig. 5). Taking into account the dimension of the flagellum, the material stiffness was calculated (5.056 ± 0.078 GPa; Fig. 4, inset). The material stiffness is almost constant irrespective of the measured position (Fig. 4, inset). Then, the estimated bending stiffness was calculated on the assumption that the material stiffness is constant in the entire flagellum (Fig. 4, dashed line). It shows a well-fitting curve to that of the measured bending stiffness (Fig. 4, solid line).

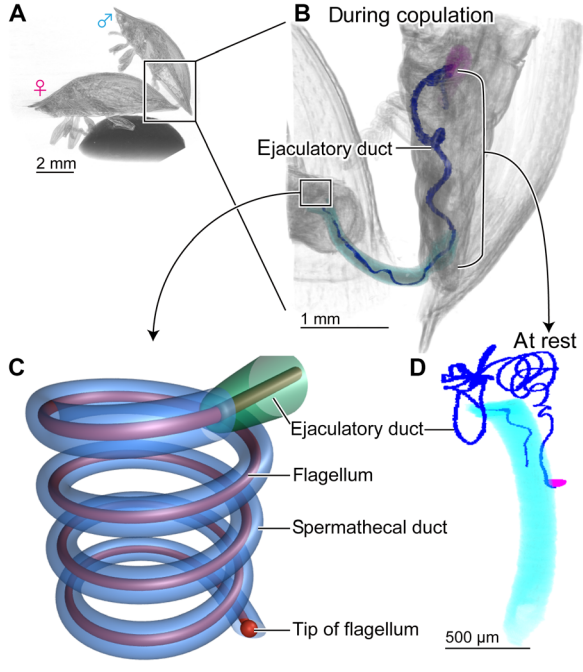


**Fig. 1. Genital morphology of *Cassida rubiginosa*.** (**A**) A couple scanned with micro–computed tomography. (**B**) An enlarged image of the abdomen during copulation; different parts of the male reproductive system are shown with different colors. (**C**) A scheme of the flagellum inserted into the spermathecal duct. (**D**) The male genitalia at rest. The flagellum is highlighted with dark blue in (B) and (D). During copulation, a primary intromittent organ (aedeagus, light blue) is inserted in a female vagina, the ejaculatory duct is shortened due to contraction of longitudinal muscles, and the flagellum is propagated to the female spermathecal duct. Figures are modified from the study by Filippov *et al.* (*14*) for (C) and Matsumura *et al.* (*25*) for (A), (B), and (D).

### Autofluorescence composition along the flagellum tip

Autofluorescence of the flagellum was visualized with special focus on the very tip (ca. 200 μm) using a CLSM equipped with four lasers (Fig. 6). In the micrograph, we assigned colors blue, green, red, and red to emitted wavelengths of 420 to 480, ≥490, ≥560, and ≥640 nm, respectively. Fundamentally, the result is congruent with the preceding one (*14*). The visualized proximal half of the flagellum tip shows red to purple, whereas its apical half showed a different color pattern. According to Michels and Gorb (*32*), this suggests that the proximal half is homogeneously composed of sclerotized cuticle. The outer curve of the flagellum at the very tip shows a color gradient from red to green and light blue from the base to the apex, which suggests a less-sclerotized cuticle. The inner side of the flagellum tip shows a homogeneous blue, which suggests a nonsclerotized cuticle and dominance of resilin there.

### Material property differences between the inner and outer parts of the flagellum tip

To compare the material properties among regions on the flagellum tip, we investigated the surfaces of the sample dried at room temperature (Fig. 7) and compared it with the one dried at critical point (*25*). The inner side of the curved tip in the scanning electron microscopy (SEM) image shows a slightly rough pattern, presumably due to some shrinkage, on the surface of a sample dried at room temperature (Fig. 7, B and C), which does not occur in samples dried at the critical point (*25*). These differences are not observed in other areas of the flagellum (for example, the apical region but not on the tip; Fig. 7, D and E).

## DISCUSSION

Bending stiffness gradient of a hyper-elongated part of the intromittent organ, the flagellum, was experimentally tested for the first time as presented in this paper. We demonstrated that the basal half of the flagellum is relatively stiff and the apical half is softer. Previously, we numerically demonstrated that flagellum performance during the penetration process is the fastest in the beetle genitalia with the presence of this type of gradient (*14*).

The relatively low bending stiffness of the flagellum's apical part is advantageous for the flagellum, allowing it to fit into the strongly spiraled spermathecal duct of the female. On the other hand, the relatively high bending stiffness of the rest of the flagellum enables it to efficiently transfer the penetration force applied to the proximal end of the flagellum (*25*). Moreover, during copulation, only the apical one-third of the flagellum is inserted, maximally, into the highly spiraled spermathecal duct (*25*). It is reasonable that only the apical part of the flagellum is relatively soft. The spermathecal duct is possibly well sclerotized, and there is a little space between the flagellum and the inner wall of the spermathecal duct during copulation (Fig. 1C) [Fig. 8 in the study by Matsumura *et al.* (*25*)]. Therefore, the spermathecal duct does not act as a perfect guide for flagellum penetration, and fitting the flagellum into the spiral shape of the female duct would be as important as completely preventing buckling in the apical region of the flagellum. In contrast to the apical part, the rest of the flagellum is situated in the lumen of the

ejaculatory duct during the entire time of copulation. The duct is membranous and presumably softer than the flagellum (*25*). Therefore, for the remaining part of the flagellum, prevention of buckling must be of high importance.

The bending stiffness gradient is produced only by the shape of the flagellum, not by the material stiffness gradient. The flagellum, except for the very tip, is likely to consist mainly of a chitinous cuticle material (*14*, *25*). Material stiffness of the arthropod cuticle, consisting of chitin nanofibers and protein matrix, changes tremendously depending on the water content [summarized in the study by Vincent and Wegst (*33*)]. However, the apparent fit between the calculated curve of bending stiffness with the assumption of the constant Young's modulus and the experimentally measured bending stiffness (Fig. 4) demonstrates that the area moment of inertia differs along the flagellum, and this in turn results in a bending stiffness gradient. The flagellum diameter and wall thickness become smaller in the apical part of the flagellum.

The Young's modulus (ca. 5 GPa) of the flagellum, except for the nonmeasured very tip, are as high as the typical tanned cuticle, whose Young's modulus vary from less than $1 \times 10^{-4}$ GPa to nearly 100 GPa (*31*). Our experimentally obtained value is comparable to wood parallel to grain, the density of which is much lower than that of the insect cuticle (*33*, *34*). The force, which is applied to the end of the flagellum for penetration, is roughly estimated at ca. 0.034 to 1.35 mN based on preceding mechanical studies on insect muscles. The force was estimated by a cross-sectional area of the longitudinal muscles [1682 $\mu m^2$, based on Fig. 3F in the study by Matsumura *et al.* (*25*) with the aid of Fiji software (*35*)] times the maximum force obtained from previous measurements on insect muscles, 2 to 80 $N/cm^{-2}$ [(*36*) and references therein]. Although the estimated pushing forces have a huge range of variations, in any case, the Young's modulus of the flagellum cuticle is big enough to convey the propulsion force efficiently to the tip without compression.

For the three-point bending test, the very tip (ca. 200 μm) had to be fixed with an insect pin (Fig. 2; see the Materials and Methods section for the setup of the bending test) using glue, and the flagellum stiffness was not directly measured. However, the result of the reanalysis of the material composition of the flagellum tip using a new sample by applying a CLSM method (*37*) strongly suggests that the inner curve of the flagellum tip is dominated by the rubber-like protein resilin (*32*, *37*). The resilin-dominated inner curve must be softer than the outer curve, because deformation of an air-dried sample occurs only in the inner curve of the flagellum tip but not in the outer curve. This is also supported by a previous study dealing with similar cuticular fibrous structures, in which the authors demonstrated that material stiffness of a resilin-dominated region is much softer than a chitin-dominated region (*38*). This material distribution found in the flagellum tip might make it tougher, because it is known that a sclerotized cuticle layer with an unsclerotized cuticle layer added to the tensile surface can store higher elastic strain energy before failure [summarized in the study by Vincent and Wegst (*33*)]. In the case of the beetle studied here, the inner surface of the female spermathecal duct is likely well sclerotized (*14*, *25*), meaning it can be harder than or comparable to the flagellum. Considering physical interactions of the male and female structures during copulation, the flagellum tip mainly receives mechanical resistance due to contacts with the spermathecal duct walls. Therefore, the flagellum tip is always exposed to the danger of breakage. Dougherty and Shuler (*27*) previously revealed such natural breakage of the flagellum-like intromittent organ in a seed bug species, *Lygaeus simulans* (Heteroptera: Lygaeidae), and showed that the fractures occurred mainly at the tip. In addition to the difference in material stiffness, the initially curved, softer tip would reduce the probability of being crushed between the flagellum tip and the spermathecal duct wall. The homogeneously circular cross sections of the flagellum may also help the flagellum tip in fitting into the highly spiraled spermathecal duct by twisting the entire flagellum, because structures with circular cross sections have relatively low ratios of bending stiffness to torsion stiffness (*39*).

Only a few biomechanical studies were carried out to understand the penetration mechanism of a hyper-elongated intromittent organ in insects, despite the fact that these structures represent a widespread phenomenon (*2*). Here, we obtained three main findings. (i) Bending stiffness becomes smaller toward the apical part, which allows the

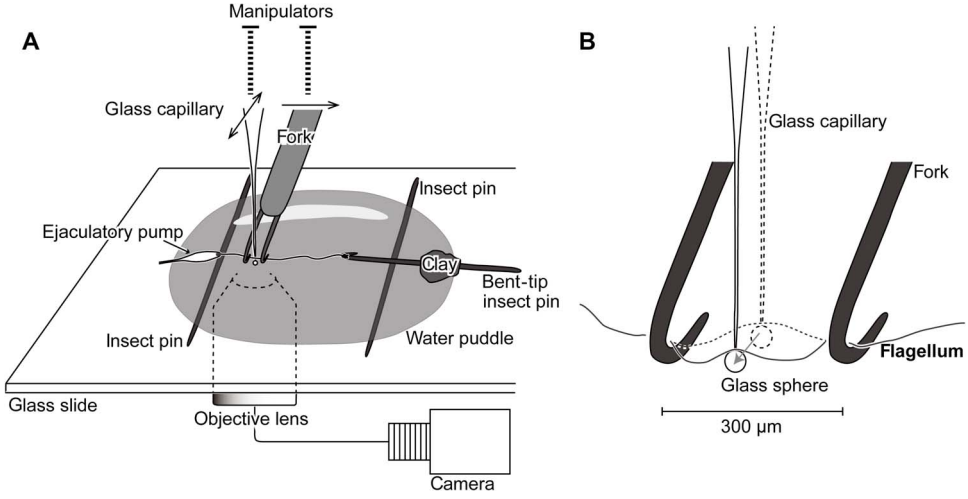


**Fig. 2. Scheme of the experimental design of the bending test.** (**A**) Setup of the bending test apart from the manipulators and the microscope. The flagellum is sunk in the water puddle, and the left end of the flagellum is fixed on the bent tip of an insect pin. The fork is set perpendicular to the flagellum and is moved toward the direction of the arrow on the fork. The glass capillary is set perpendicular to the fork and flagellum. The glass capillary is movable in the direction of the arrows on the glass capillary. (**B**) An enlarged scheme of the bent flagellum. The insect pins at a distance of 300 μm from each other compose the fork. The glass capillary is set behind the flagellum and was movable forward (the arrow) to bend the flagellum.

flagellum to easily fit to the shape of the spermathecal duct. (ii) The very tip comprises softer and harder sides running parallel to each other; this presumably makes the tip tougher. (iii) The very tip curls up initially, and the cross section of almost the entire flagellum is cylindrical; this helps the very tip to fit to the complex shape of the spermathecal duct. These findings can be potentially applicable for other animals.

For vertebrate animals, there are plenty of mechanical studies related to penis penetration and erection [for example, in the studies by Kelly (*30*, *40*, *41*)], including human beings from a medial point of view [reviewed by Udelson (*20*)]. Penetration and erection mechanisms strongly vary in vertebrates (*30*); however, in any case, avoiding buckling is critically important. For example, it is known that men having a penis that easily buckles often fail in penetration (*20*). In addition, an axial orthogonal array of collagen fibers reinforces the penis, resisting bending during copulation in cases of inflatable penises (*41*). Buckling of penises depends on penetration force magnitude, axial resistive force by females, vaginal size, and existence of lubrication (*20*).

In the case of insects, none of the proposed hypotheses on penetration of the hyper-elongated part of the intromittent organ hold: Insertion is

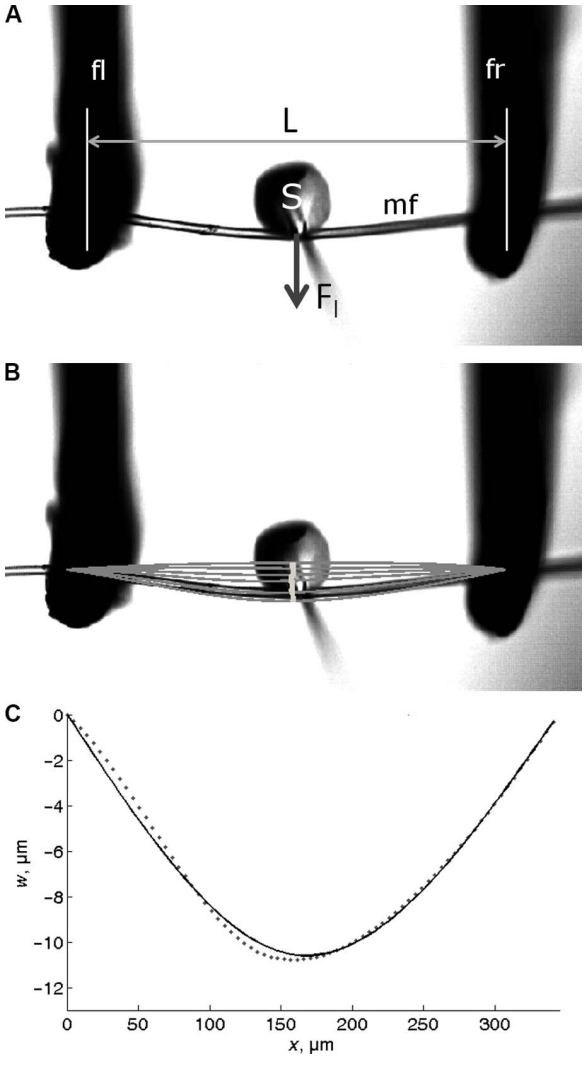


**Fig. 3. Bending experiment.** The images (**A**) and (**B**) were taken from the bottom of the setup of the bending test shown in Fig. 2. The glass capillary with the glass sphere was moved from the upper to the lower side of each image. (A) A glass capillary terminated with a glass sphere (S) produces a load ($F_l$) on a fragment of the male flagellum (mf), which rests on a fork (fl, fork left; fr, fork right). (B) The trajectory of the sphere motion is shown with a thick light gray line. The flagellum at different loads is shown as a series of the gray lines. (**C**) Theoretical (solid line, calculated according to Eq. 1) and experimental (dotted line) deformation curves of flagellum deformation at 2.56 μN loading force. *w* (*y* axis) represents the deformation at position *x*.

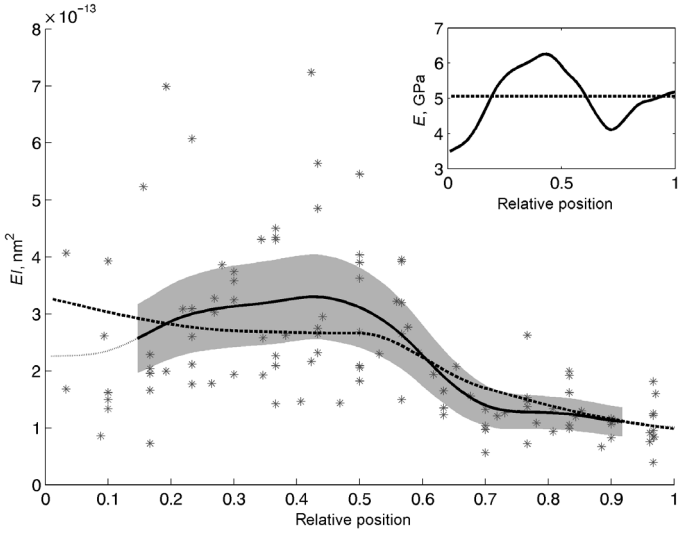


**Fig. 4. Flexural rigidity of the flagellum of *C. rubiginosa*.** Individual values of flexural rigidity are shown as asterisks. The smoothed values of flexural rigidity are shown as a black solid line within the range, where the SE was calculated (SE is shown as a gray area), and outside that range as a dark gray line . The effective Young's modulus calculated from the smoothed flexural rigidity curve is shown in the inset as a solid black line. A dashed line in the inset corresponds to a constant effective Young's modulus (independent on the location), the value of which was used to calculate the flexural rigidity curve shown as a black dashed line in the main figure.

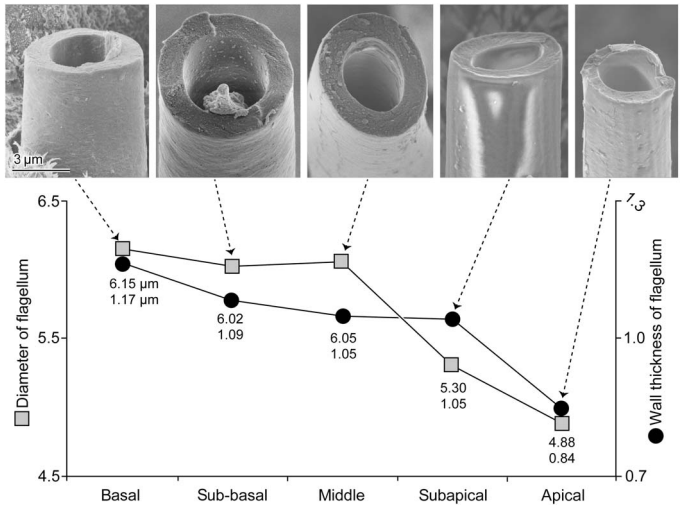


**Fig. 5. The flagellum measurements of *C. rubiginosa* with representative SEM images.** The upper values in the graph represent the diameters of the flagellum on an average, and the lower values represent the wall thickness of the flagellum on an average. The material situated on the inner wall of the flagellum at the subbasal region is likely debris of sperm.

made by using rather small muscle contractions instead of using entire body movements (*2*, *25*, *42*–*45*). Therefore, the interactions of the flagellum with corresponding female structures play an even more important role in insects. The spermathecal duct of the studied species is surrounded by soft tissue (*25*), which presumably produces a specific secretion, known from other insects [reviewed by Pascini and Martins (*46*)]. The original function of such a secretion is maintenance of sperm viability (*46*); however, it should also work as a lubrication mechanism for flagellum penetration. In general, studies of the female genital system are far fewer in comparison to those of males (*47*), and we do not have any relevant mechanical information on the female genitalia. It is very challenging, however, to evaluate obtained data on, for example, Young's modulus and bending stiffness of female structures and viscosity of female secretion, but they should also be investigated to understand the functions of genitalia.

Other types of insertion with elongated structures in nature are, as were introduced in the beginning of the present paper, female ovipositors and insect mouthparts. Mechanical properties, which are comparable to the current study, have been reported only in some studies (*48*–*50*). Kundanati and Gundiah (*49*) directly measured the material stiffness of the ovipositor of a fig wasp. From the figures they presented, the ovipositor size seems to be comparable to the beetle flagellum, and the Young's modulus is 1.42 ± 0.29 GPa in the very tip and 0.73 ± 0.19 GPa in a remote region (*49*). Contrary to the intuitive thought that flagellum penetration occurring in a preexisting spermathecal duct is an easier task than a "drilling" type of insertion, their Young's modulus are smaller than those of the beetle we studied, despite the presence of zinc in the ovipositor tip (*49*). This suggests that the measured material stiffness of the flagellum and ovipositor is more important for transferring penetration force from the base to the tip than for drilling plant substrates. It does not mean that the material stiffness does not matter for drilling, because stiffness (in newton per meter) of the ovipositors in damselflies and dragonflies vary among species, although it does not always correspond to the preferred substrate stiffness (*48*, *50*).

Considering certain functional similarity between the biological system of the beetle penis and medical catheters in terms of insertions of long and thin ducts into narrow spaces, our results could provide us with some hints for further technical improvement of existing catheters. The biggest drawback of catheter use is possible health complications caused by different factors [for example, (*51*–*54*)]. As one of the factors, inaccurate catheter tip location is discussed (*51*, *54*). Although there are constraints for changes of the catheters' design due to the complexity and diversity of catheter usage, the self-controlling system of the beetle flagellum position can be potentially applicable for it. Our results revealed that shape, bending stiffness, and Young's modulus of materials of future medical catheters along the length should be taken into account and a gradient of their mechanical properties should be carefully considered. To apply the design principles of the studied biological system for catheters, we have to understand our biological system in further detail in the future. For example, the visualization of genital interactions and its quantitative analyses of the flagellum during the insertion process are mandatory. Filming of beetle genital movement using synchrotron-based in vivo x-ray cineradiography (*55*) should be applied as a next step. This paper concludes that the experimental and theoretical works on biomechanics of insertion of elongated structures have just started, and we expect more comparative data in the near future. This will be essential for the further understanding of this fascinating biomechanical system that is highly important not only for evolutionary biology but also for the future development of medical devices.


**Fig. 6. CLSM image of the flagellum tip of *C. rubiginosa*.** We assigned colors blue, green, red, and red to emitted wavelengths of 420 to 480, ≥490, ≥560, and ≥640 nm, respectively.

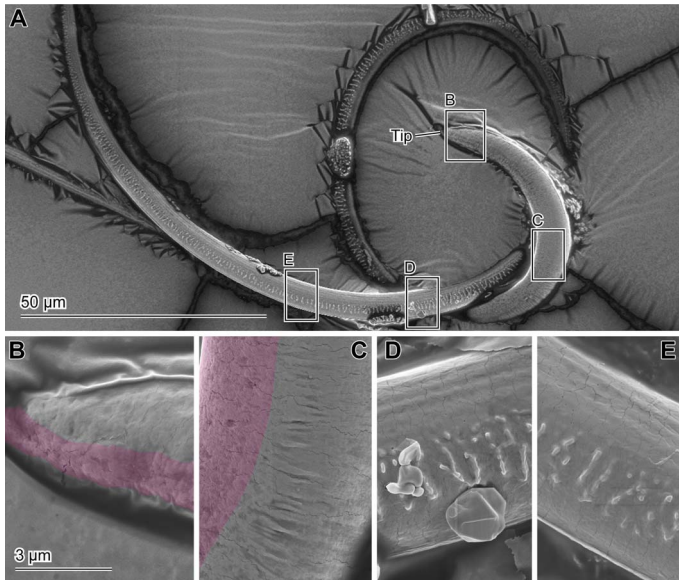


**Fig. 7. SEM images of the flagellum of *C. rubiginosa*.** (**A**) Map of the images below, the tip of the flagellum. (**B** to **E**) Enlarged images of the flagellum corresponding to the squares in (A). The pink-colored areas in (B) and (C) represent shrunk surfaces. The scale bar in (B) is applicable for (C) to (E).

## MATERIALS AND METHODS

### Sample collection and preparation

The beetles, *C. rubiginosa*, were collected in Jena, Germany, and kept in plastic boxes together with the plant *Cirsium* spp. (Asteraceae). Beetles collected in the wild were used for the following bending test. Other beetles collected in the field as well as beetles raised in laboratories were used for other experiments. Carbon dioxide–anesthetized beetles were dissected in phosphate-buffered saline (PBS; Carl Roth GmbH & Co. KG) under a stereomicroscope (Olympus SZX12, Olympus Corporation) when fresh flagella were essential. We then transferred the dissected flagella into distilled water that was further used as a medium for the bending test. Completing an experiment on a single individual took 2 to 3 hours. To avoid a change in the concentration of chemical substances in the medium during the experiment, we used distilled water as the medium instead of PBS. Because the flagellum largely consists of a chitinous cuticle material (*25*), its stiffness markedly changes depending on water content, similar to other cuticular structures (*33*, *38*).

### Bending test

To measure bending stiffness and material properties of the flagellum, we applied a bending test for several sites on the flagellum. First, we prepared two tools: a fork for flagellum support and a glass capillary as a force transducer (Fig. 2A). The fork consisted of two Austerlitz Insect Pins (0.01 mm in diameter; Entomoravia), whose tips were bent to hook the flagellum. The bent-tip insect pins were fixed on a plastic rod. The distance between the insect pins was adjusted to ca. 300 µm with the aid of a micrometer (Fig. 2B). The glass capillary was prepared by pulling a thin-wall borosilicate glass capillary (120 × 1 mm; Hirschmann-Laborgeräte GmbH &Co. KG) using a pipette puller (H. Saur Laborbedarf). A glass sphere (ca. 50 µm in diameter) was glued with super glue to the capillary tip. A glass capillary, whose bending flexibility was comparable to that of the flagellum, was selected for further experiments to be used as a force transducer after its calibration using a balance as described below. The fork and a selected glass capillary were firmly fixed on standard manual control micromanipulators (MM-33) (Warner Instruments LLC) and a three-axial nano- and micropositioning system (F-130, Physik Instrumente GmbH & Co. KG), respectively. The first manipulator was fixed on a stable metal pillar and mounted on an inverted microscope (Axio Observer A1, Carl Zeiss MicroImaging GmbH). The second manipulator was directly fixed on the microscope. The motion of the glass capillary and the flagellum deformation were recorded using a camera (Basler piA1900-32g, Basler Vision Technologies) and the software StreamPix 5 (NorPix Inc.) attached to the C-mount connector on the microscope.

The entire reproductive system was carefully dissected in PBS from freshly killed beetles, and the epidermis and muscles of the ejaculatory duct and the testes were carefully removed from the male reproductive system. Only the flagellum with an ejaculatory pump was used for further experiments. For the experiment, we used 10 males in total. The flagellum was placed, in distilled water, onto a cover glass (Fig. 2), which was then placed onto the inverted microscope. Then, we mechanically hooked the ejaculatory pump onto the insect pin on the left side (Fig. 2A) to prevent the flagellum from floating on the water's surface. By using two parallel arranged insect pins, including the left pin, we avoided touching the flagellum with the coverslip during the bending test. The distal part of the ejaculatory pump was placed partly out of the water, which worked as sort of a glue after being dried. Then, we glued the tip of the flagellum to the bent tip of another insect pin using polyvinylsiloxane (PVS) (Coltène/Whaledent AG), the bent-tip insect pin was placed on the insect pin located on the right side, and the insect pin was stabilized with a small amount of clay. Because the tip of the flagellum of the studied species is often coiled, the hook of the bent tip of the insect pin was able to hook mechanically, at least temporarily, and the PVS made the connection stable. However, the PVS was not always used because of the tight mechanical binding between the bent-tip insect pin and the coiled tip of the flagellum.

We carefully moved the bent-tip insect pin with the flagellum tip to make the flagellum nearly linear, but never being stretched. Then, the fork was placed perpendicular to the flagellum, and the glass capillary was placed perpendicular to the fork and flagellum and in-between was the bent-tip insect pins of the fork. Then, with the aid of the micromanipulator connected to the glass capillary, we moved the glass capillary forward to bend the section of the flagellum between the fork with a step size of 20 µm and a velocity of 100 µm/s. We took a photo of each step, which were later used to analyze the successive performance of the flagellum during bending. This experiment was conducted from the base of the flagellum first and was performed every second 300-µm section along the flagellum to the tip. Using this method, we performed the bending test from 13 to 17 sections for each individual depending on the flagellum length.

After all the tests, the glass capillary of the abovementioned setup was calibrated using the ultramicrobalance MT-SICS-UMX2 (Mettler Toledo GmbH) following the methods developed in preceding studies [for example, (*56*–*58*)] [see Fig. 5B in the study by Wolff *et al.* (*56*)]. In brief, the glass capillary attached to the manipulator was carefully moved to the ultramicrobalance. We prepared a small glass shell, on which a piece of a razor blade was glued perpendicular to the glass with super glue, and then placed it on the stage of the ultramicrobalance. The glass capillary was approached toward the blade from above, carefully with the aid of a binocular. Then, from a few steps before contact to the blade, we recorded the number of moved steps of the glass capillary and the weight loaded on the microbalance through the blade.

### Data analyses and numerical simulation

For the determination of the bending force, the trajectory of the capillary tip with the glass sphere on it was digitalized. The displacement of the sphere was determined using two-dimensional correlation function between two consecutive images within the mask determined at the beginning of the series (Fig. 3, A and B). The loading force ($F_l$) was calculated as a product of the glass capillary deformation $\Delta x$ and the spring constant of the glass capillary ($k_c$). Flexural rigidity and Young's modulus were calculated from the fitting of deformation curves (Fig. 3, B and C) by using the following equations for small deflections (*59*)

$$\begin{cases} w = \dfrac{F_l(L-a)x}{6EIL}\left(x^2 - 2La + a^2\right), x < \alpha \\ w = \dfrac{F_l a(L-x)}{6EIL}\left(x^2 - 2Lx + a^2\right), x > \alpha \end{cases} \quad (1)$$

where $L$ is the width of the fork, $a$ is the position of the applied load, $w$ is the deformation at position $x$, and $EI$ is the flexural rigidity. For the calculation of Young's modulus, the flagellum was considered as a cylinder with a radius of 5 µm and a wall thickness of 1.5 µm. The second moment of area ($I$) was calculated, according to a classic formula for a tube [for example, see the study by Jones *et al.* (*59*)]

$$I = (\pi/4)\left(r^4 - (r-t)^4\right) \quad (2)$$

where $r$ and $t$ are the outer radius and the wall thickness of the male flagellum. These parameters were estimated on the basis of the measurements presented in Fig. 5 and interpolated in other locations with third-order polynomial.

The smoothed flexural rigidity was calculated to minimize the following expression [similar to the study by Kreitschitz *et al.* (*60*)]: $|\mathbf{f} - A\mathbf{f}_s|^2 + \lambda^2|D\mathbf{f}_s|^2$, where $\mathbf{f}$ and $\mathbf{f}_s$ are the flexural rigidity values obtained from the experiment and smoothed values, respectively, $A$ is a linear interpolation matrix, $D$ is a matrix for the calculation of a second derivative, and $\lambda$ is a regularization parameter. The lowest value of the regularization parameter ($\lambda = 3 \times 10^{-16}$) was selected, and by that, $\mathbf{f}_s$ had just one maximum (Fig. 4, black thick line).

The SE in Fig. 4 was calculated within a running window over 20 individual measurements relative to $\mathbf{f}_s$. Young's modulus of the walls of the flagellum was calculated in two different ways. It was assumed to be either dependent on or independent of the location on the flagellum.

### Confocal laser scanning microscopy

By visualizing the autofluorescence of the flagellum to estimate material compositions, we investigated the flagellum using the CLSM Zeiss LSM 700 (Zeiss) with 20× objective lens (Zeiss Plan-Apochromat; numerical aperture, 0.8). A flagellum freshly dissected in PBS was visualized according to Michels and Gorb (*32*). Briefly, the sample was embedded in glycerin as a medium on a glass slide 1 hour before visualization to stabilize the sample in the medium. Then, we used 405-, 488-, 555-, and 639-nm laser lines for excitation wavelengths and applied a band-pass emission filter 420 to 480 nm and long-pass emission filters transmitting light with wavelengths of ≥490, ≥560, and ≥640 nm, respectively. Then, we visualized the emitted wavelengths 420 to 480, ≥490, ≥560, and ≥640 nm by assigning blue, green, red, and red, respectively, in the final image. The final image was adjusted for contrast and brightness using the software Adobe Photoshop Elements 9 (Adobe Systems).

### Scanning electron microscopy

Quantifying the flagellum size variations along its length, we used two males fixed and preserved in 70% ethanol. The flagella were carefully dissected out and gradually dehydrated with an ascending ethanol series up to 100%. Then, they were dried with the critical point dryer CPDA (Quorum Technologies Ltd.). The flagella were first broken into five regions (basal, sub-basal, middle, subapical, and apical) using fine tweezers. Each region was broken into small pieces and mounted on adhesive carbon sheets in a way to show the transverse plane of the broken flagella. Then, the samples were sputter-coated with gold-palladium (ca. 10-nm thickness) using the Leica EM SCD500 high-vacuum sputter coater (Leica Microscopy GmbH) and visualized with the SEM Hitachi S-4800 (Hitachi High-Tech Corp.) at an accelerating voltage of 3 kV. Micrographs of all visible transversal planes of the broken flagella were taken. The micrographs were used for measuring the outer diameter and flagellum wall thickness with the aid of the Fiji software (*35*). Deformation was not preventable through the flagellum breaking process, and also preparing a perfect transverse plane of the flagella was almost impossible. Therefore, we measured the diameter only for the flagellum pieces plausibly without deformation and the wall thickness from where the surface was apparently flat. We measured the wall thickness maximum for two sites from each piece of the flagellum, if it was possible.

Estimating the stiffness differences between the internal and external curves of the flagellum tip caused by material composition differences, we used not only CLSM but also SEM. A freshly dissected flagellum was placed in a plastic case overnight and dried at room temperature. Then, the surface of the sample was visualized with the abovementioned methods.

## SUPPLEMENTARY MATERIALS

Supplementary material for this article is available at http://advances.sciencemag.org/cgi/content/full/3/12/eaao5469/DC1

table S1. Flexural rigidity of the flagellum of *C. rubiginosa*.
table S2. Measurements of the flagellum wall thickness of *C. rubiginosa* (average ± SD).
table S3. Measurements of the flagellum diameter of *C. rubiginosa* (average ± SD).

## REFERENCES AND NOTES


1. C. J. Neufeld, A. R. Palmer, Precisely proportioned: Intertidal barnacles alter penis form to suit coastal wave action. *Proc. R. Soc B.* **275**, 1081–1087 (2008).
2. Y. Matsumura, K. Yoshizawa, R. Machida, Y. Mashimo, R. Dallai, M. Gottardo, T. Kleinteich, J. Michels, S. N. Gorb, R. G. Beutel, Two intromittent organs in *Zorotypus caudelli* (Insecta, Zoraptera): The paradoxical coexistence of an extremely long tube and a large spermatophore. *Biol. J. Linn. Soc.* **112**, 40–54 (2014).
3. G. D. Weiblen, How to be a fig wasp. *Annu. Rev. Entomol.* **47**, 299–330 (2002).
4. W.-Q. Zhen, D.-W. Huang, J.-H. Xiao, D.-R. Yang, C.-D. Zhu, H. Xiao, Ovipositor length of three *Apocrypta* species: Effect on oviposition behavior and correlation with syconial thickness. *Phytoparasitica* **33**, 113–120 (2005).
5. J. Hughes, A. P. Vogler, Ecomorphological adaptation of acorn weevils to their oviposition site. *Evolution* **58**, 1971–1983 (2004).
6. H. W. Krenn, Feeding mechanisms of adult Lepidoptera: Structure, function, and evolution of the mouthparts. *Annu. Rev. Entomol.* **55**, 307–327 (2010).
7. F. Karolyi, J. F. Colville, S. Handschuh, B. D. Metscher, H. W. Krenn, One proboscis, two tasks: Adaptations to blood-feeding and nectar-extracting in long-proboscid horse flies (Tabanidae, *Philoliche*). *Arthropod Struct. Dev.* **43**, 403–413 (2014).
8. A. Ahmad, S. Kaushik, V. V. Ramamurthy, S. Lakhanpaul, R. Ramani, K. K. Sharma, A. S. Vidyarthi, Mouthparts and stylet penetration of the lac insect *Kerria lacca* (Kerr) (Hemiptera:Tachardiidae). *Arthropod Struct. Dev.* **41**, 435–441 (2012).
9. J. Brożek, E. Mróz, D. Wylężek, Ł Depa, P. Węgierek, The structure of extremely long mouthparts in the aphid genus *Stomaphis* Walker (Hemiptera: Sternorrhyncha: Aphididae). *Zoomorphology* **134**, 431–445 (2015).
10. V. Rodriguez, D. M. Windsor, W. G. Eberhard, Tortoise beetle genitalia and demonstrations of a sexually selected advantage for flagellum length in Chelymorpha alternans (Chrysomelidae, Cassidini, Stolaini), in *New Developments in the Biology of Chrysomelidae*, P. Jolivet, J.A. Santiago-Blay, M. Schmitt, Eds. (SPB Academic Publisher, 2004), pp 739–748.
11. K. Ilango, R. P. Lane, Coadaptation of male aedeagal filaments and female spermathecal ducts of the old world Phlebotomine sand flies (Diptera: Psychodidae). *J. Med. Entomol.* **37**, 653–659 (2000).
12. Y. Matsumura, I. Yao, R. G. Beutel, K. Yoshizawa, Molecular phylogeny of the leaf beetle subfamily Criocerinae (Coleoptera: Chrysomelidae) and the correlated evolution of reproductive organs. *Arthropod Syst. Phylogeny* **72**, 95–110 (2014).
13. A. Filippov, A. Kovalev, Y. Matsumura, S. N. Gorb, Male penile propulsion into spiraled spermathecal ducts of female chrysomelid beetles: A numerical simulation approach. *J. Theor. Biol.* **384**, 140–146 (2015).
14. A. E. Filippov, Y. Matsumura, A. E. Kovalev, S. N. Gorb, Stiffness gradient of the beetle penis facilitates propulsion in the spiraled female spermathecal duct. *Sci. Rep.* **6**, 27608 (2016).
15. S. S. Singh, M. A. Jansen, N. M. Franz, N. Chawla, Microstructure and nanoindentation of the rostrum of *Curculio longinasus* Chittenden, 1927 (*Coleoptera: Curculionidae*). *Mater Charact* **118**, 206–211 (2016).
16. M. A. Jansen, S. S. Singh, N. Chawla, N. M. Franz, A multilayer micromechanical model of the cuticle of *Curculio longinasus* Chittenden, 1927 (Coleoptera: Curculionidae). *J. Struct. Biol.* **195**, 139–158 (2016).
17. U. Cerkvenik, B. van de Straat, S. W. S. Gussekloo, J. L. van Leeuwen, Mechanisms of ovipositor insertion and steering of a parasitic wasp. *Proc. Natl. Acad. Sci. U.S.A.* **114**, E7822–E7831 (2017).
18. E. Parle, S. Herbaj, F. Sheils, H. Larmon, D. Taylor, Buckling failures in insect exoskeletons. *Bioinspir. Biomim.* **11**, 016003 (2015).
19. A. Sakes, D. Dodou, P. Breedveld, Buckling prevention strategies in nature as inspiration for improving percutaneous instruments: A review. *Bioinspir. Biomim.* **11**, 021001 (2016).
20. D. Udelson, Biomechanics of male erectile function. *J. R. Soc. Interface* **4**, 1031–1047 (2007).
21. R. E. Snodgrass, *Principles of Insect Morphology* (McGraw-Hill Book Co., 1935).
22. R. Gschwentner, A. Tadler, Functional anatomy of spermatheca and its duct in the seed bug *Lygaeus simulans* (Heteroptera: Lygaeidae). *Eur. J. Entomol.* **97**, 305–312 (2000).

23. Y. Kamimura, Possible removal of rival sperm by the elongated genitalia of the earwig, *Euborellia plebeja*. *Zool. Sci.* **17**, 667–672 (2000).
24. Y. Matsumura, S.-I. Akimoto, Mating behavior and genital damage during copulation in the leaf beetle *Lema coronata* (Chrysomelidae: Criocerinae). *Entomol. Sci.* **12**, 215–217 (2009).
25. Y. Matsumura, J. Michels, E. Appel, S. N. Gorb, Functional morphology and evolution of the hyper-elongated intromittent organ in *Cassida* leaf beetles (Coleoptera: Chrysomelidae: Cassidinae). *Zoology* **120**, 1–14 (2017).
26. Y. Kamimura, Y. Matsuo, A "spare" compensates for the risk of destruction of the elongated penis of earwigs (Insecta: Dermaptera). *Naturwissenschaften* **88**, 468–471 (2001).
27. L. R. Dougherty, D. M. Shuker, Natural breakage of the very long intromittent organ of the seed bug *Lygaeus simulans* (Heteroptera: Lygaeidae). *Eur. J. Entomol.* **112**, 818–823 (2015).
28. L. R. Dougherty, I. A. Rahman, E. R. Burdfield-Steel, E. V. Greenway, D. M. Shuker, Experimental reduction of intromittent organ length reduces male reproductive success in a bug. *Proc. R Soc. B* **282**, 20150724 (2015).
29. P. L. R. Brennan, Studying genital coevolution to understand intromittent organ morphology. *Integr. Comp. Biol.* **56**, 669–681 (2016).
30. D. A. Kelly, Intromittent organ morphology and biomechanics: Defining the physical challenges of copulation. *Integr. Comp. Biol.* **56**, 705–714 (2016).
31. M. Burns, J. W. Schultz, Mechanical properties of male genitalia in *Leiobunum* harvestmen (Opiliones: Sclerosomatidae). *J. Arachnol.* **44**, 199–209 (2016).
32. J. Michels, S. N. Gorb, Detailed three-dimensional visualization of resilin in the exoskeleton of arthropods using confocal laser scanning microscopy. *J. Microsc.* **245**, 1–16 (2012).
33. J. F. V. Vincent, U. G. K. Wegst, Design and mechanical properties of insect cuticle. *Arthropod Struct. Dev.* **33**, 187–199 (2004).
34. U. G. K. Wegst, M. F. Ashby, The mechanical efficiency of natural materials. *Philos. Mag.* **84**, 2167–2186 (2004).
35. J. Schindelin, I. Arganda-Carreras, E. Frise, V. Kaynig, M. Longair, T. Pietzsch, S. Preibisch, C. Rueden, S. Saalfeld, B. Schmid, J.-Y. Tinevez, D. J. White, V. Hartenstein, K. Eliceiri, P. Tomancak, A. Cardona, Fiji: An open-source platform for biological-image analysis. *Nat. Methods* **9**, 676–682 (2012).
36. J. Goyens, J. Dirckx, M. Dierick, L. Van Hoorebeke, P. Aerts, Biomechanical determinants of bite force dimorphism in *Cyclommatus metallifer* stag beetles. *J. Exp. Biol.* **217**, 1065–1071 (2014).
37. J. Michels, E. Appel, S. N. Gorb, Functional diversity of resilin in arthropoda. *Beilstein J. Nanotechnol.* **7**, 1241–1259 (2016).
38. H. Peisker, J. Michels, S. N. Gorb, Evidence for a material gradient in the adhesive tarsal setae of the ladybird beetle *Coccinella septempunctata*. *Nat. Commun.* **4**, 1661 (2013).
39. S. Vogel, Twist-to-bend ratios and cross-sectional shapes of petioles and stems. *J. Exp. Bot.* **43**, 1527–1532 (1992).
40. D. A. Kelly, Expansion of the tunica albuginea during penile inflation in the nine-banded armadillo (Dasypus novemcinctus). *J. Exp. Biol.* **202**, 253–265 (1999).
41. D. A. Kelly, The functional morphology of penile erection: Tissue designs for increasing and maintaining stiffness. *Integr. Comp. Biol.* **42**, 216–221 (2002).
42. W. G. Eberhard, Threading a needle with reinforced thread: Intromission in *Ceratitis capitata* (Diptera, Tephritidae). *Can. Entomol.* **137**, 174–181 (2005).
43. Y. Matsumura, K. Yoshizawa, Insertion and withdrawal of extremely elongated genitalia: A simple mechanism with a highly modified morphology in the leaf beetle, *Lema coronata*. *Biol. J. Linn. Soc.* **99**, 512–520 (2010).
44. R. D. Briceño, D. Orozco, J. L. Quintero, P. Hanson, M. del Refugio Hernández, Copulatory behaviour and the process of intromission in *Anastrepha ludens* (Diptera: Tephritidae). *Rev. Biol. Trop.* **59**, 291–297 (2011).
45. P. Jałoszyński, Y. Matsumura, R. G. Beutel, Evolution of a giant intromittent organ in Scydmaeninae (Coleoptera: Staphylinidae): Functional morphology of the male postabdomen in Mastigini. *Arthropod Struct. Dev.* **44**, 77–98 (2015).
46. T. V. Pascini, G. F. Martins, The insect spermatheca: An overview. *Zoology* **121**, 56–71 (2017).
47. M. Ah-King, A. B. Barron, M. E. Herberstein, Genital evolution: Why are females still understudied? *PLOS Biol.* **12**, e1001851 (2014).
48. N. Matushkina, S. Gorb, Mechanical properties of the endophytic ovipositor in damselflies (Zygoptera, Odonata) and their oviposition substrates. *Zoology* **110**, 167–175 (2007).
49. L. Kundanati, N. Gundiah, Biomechanics of substrate boring by fig wasps. *J. Exp. Biol.* **217**, 1946–1954 (2014).
50. N. Matushkina, P. Lambret, S. Gorb, Keeping the golden mean: Plant stiffness and anatomy as proximal factors driving endophytic oviposition site selection in a dragonfly. *Zoology* **119**, 474–480 (2016).
51. G.-J. van Geffen, J. Bruhn, Continuous Peripheral Nerve Blocks Safe Practice and Management, in *Complications of Regional Anesthesia*, B. Finucane, B. Tsui, Eds. (Springer, 2017), pp. 167–185.
52. J. Lockhart, A. Boyle, L. C. Kidd, B. Shah, J. Beilan, B. Allen, L. Wiegand, D. Hernandez, R. Carrion, The lotus catheter: A non-balloon novel urethral catheter - a prospective study. *J. Urol. Ren. Dis.* **2017**, J125 (2017).
53. F. Hebal, H. T. Sparks, K. L. Rychlik, M. Bone, S. Tran, K. A. Barsness, Pediatric arterial catheters: Complications and associated risk factors. *J. Pediatr. Surg.* 10.1016/j.jpedsurg.2017.08.057.
54. X. Zhang, D. Jia, N. Ke, C. Liu, L. Fu, X. Hu, Excellent inter-observer agreement between radiologist and nurse: Tracheal carina-based identification of peripherally inserted central catheter tip position. *J. Vasc. Access* 10.5301/jva.5000799.
55. N. C. Wulff, T. van de Kamp, T. dos Santos Rolo, T. Baumbach, G. U. C. Lehmann, Copulatory courtship by internal genitalia in bushcrickets. *Sci. Rep.* **7**, 42345 (2017).
56. J. O. Wolff, A. L. Schönhofer, C. F. Schaber, S. N. Gorb, Gluing the 'unwettable': Soil-dwelling harvestmen use viscoelastic fluids for capturing springtails. *J. Exp. Biol.* **217**, 3535–3544 (2014).
57. E. Kizilkan, J. Strueben, X. Jin, C. F. Schaber, R. Adelung, A. Staubitz, S. N. Gorb, Influence of the porosity on the photoresponse of a liquid crystal elastomer. *R. Soc. Open Sci.* **3**, 150700 (2016).
58. C. F. Schaber, F. G. Barth, Spider joint hair sensilla: Adaptation to proprioreceptive stimulation. *J. Comp. Physiol. A Neuroethol. Sens. Neural Behav. Physiol.* **201**, 235–248 (2015).
59. F. D. Jones, H. H. Ryffel, E. Oberg, C. J. McCauley, R. M. Heald, *Machinery's Handbook* (Industrial Press, ed. 27, 2004).
60. A. Kreitschitz, A. Kovalev, S. N. Gorb, Slipping *vs* sticking: Water-dependent adhesive and frictional properties of *Linum usitatissimum* L. seed mucilaginous envelope and its biological significance. *Acta Biomater.* **17**, 152–159 (2015).


**Acknowledgments:** We thank H. Pohl (Jena University, Germany) for his assistance in collecting *C. rubiginosa*, J. Oesert (Kiel University, Germany) for his technical help in setting up the bending test, C. Schaber and E. Kizilkan (Kiel University, Germany) for their technical help in building up the bending test experiment and bibliographic information, and V. Kastner (Germany) for the English corrections. In addition, Y.M. thanks H. Rajabi and S. Ito (Kiel University, Germany) for the daily discussions on general biomechanics. **Funding:** The study was supported through funding from the Yamada Science Foundation (for studying abroad), the Japan Society of the Promotion of Science (postdoctoral fellowship, grant no. 15J03484), the German Research Foundation (DFG grant no. MA 7400/1-1 to Y.M.), and by the CARBTRIB Project of Leverhulme to S.G. We acknowledge financial support by Land Schleswig-Holstein within the funding programme Open Access Publikationsfonds. **Author contributions:** All authors designed the research and the bending experiment, set up the bending experiment, interpreted the findings, and wrote the manuscript. Y.M. performed the bending experiment and the CLSM and SEM analysis. A.E.K. calculated the flexural rigidity and Young's modulus. **Competing interests:** The authors declare that they have no competing interests. **Data and materials availability:** All data needed to evaluate the conclusions in the paper are present in the paper and/or the supplementary tables. Additional data related to this paper may be requested from the authors.

Submitted 1 August 2017
Accepted 20 November 2017
Published 20 December 2017
10.1126/sciadv.aao5469

**Citation:** Y. Matsumura, A. E. Kovalev, S. N. Gorb, Penetration mechanics of a beetle intromittent organ with bending stiffness gradient and a soft tip. *Sci. Adv.* **3**, eaao5469 (2017).